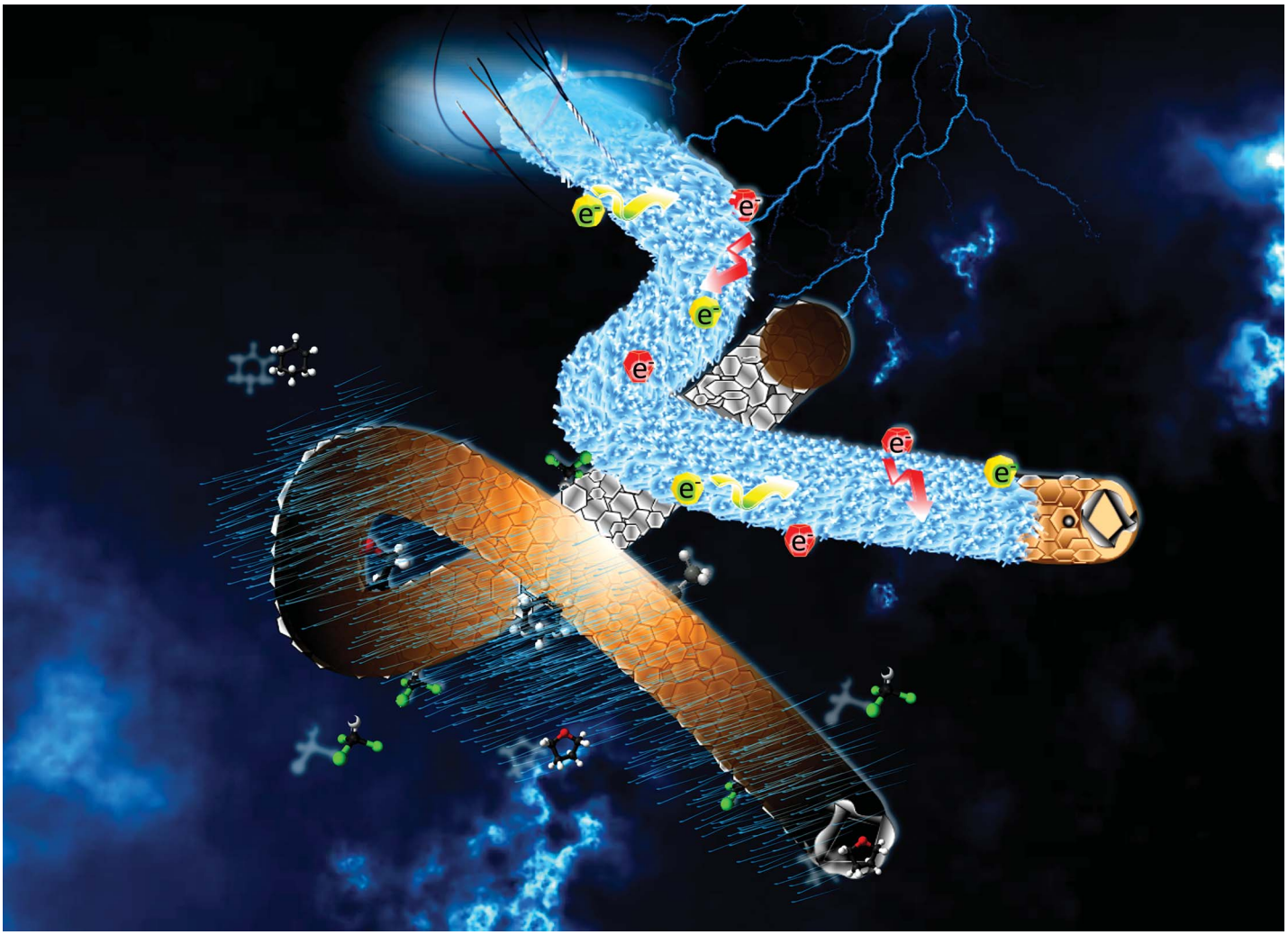

Guidelines to fabricate fiber-based organic vapor sensors based on polymer composites *via* wet spinning and modification of any "off-the-shelf fiber" *via* electrospinning for simultaneous power storage by Associate Prof. Shengyuan Yang and Prof. Meifang Zhu at the State Key Laboratory for Modification of Chemical Fibers and Polymer Materials (SKLFPM), Donghua University.

A bottom-up approach to design wearable and stretchable smart fibers with organic vapor sensing behaviors and energy storage properties

Stretchable poly(styrene-butadiene-styrene)/few-layer graphene composite (SBS-G) fibers with high sensitivity and excellent reversibility, as well as fast response to both polar and non/low-polar organic vapors were obtained. The modified SBS-G fiber coated with electroactive carbon black (CB) nanofibers showed an excellent capacitive performance, high energy and power density values.

As featured in:

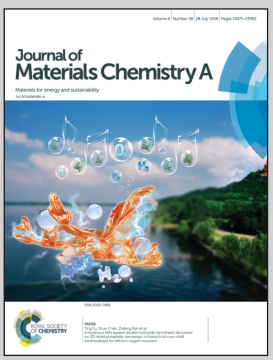

See Shengyuan Yang, Meifang Zhu *et al.*, *J. Mater. Chem. A*, 2018, **6**, 13633.

ROYAL SOCIETY OF CHEMISTRY

rsc.li/materials-a

Journal of Materials Chemistry A

PAPER

View Article Online
View Journal | View Issue

Cite this: J. Mater. Chem. A, 2018, 6, 13633

A bottom-up approach to design wearable and stretchable smart fibers with organic vapor sensing behaviors and energy storage properties†

Ifra Marriam, ‡[a] Xingping Wang,‡[a] Mike Tebyetekerwa, [ab] Guoyin Chen,[a] Fatemeh Zabihi,[a] Jürgen Pionteck, [c] Shengjie Peng,[d] Seeram Ramakrishna, [d] Shengyuan Yang *[a] and Meifang Zhu *[a]

Received 10th April 2018
Accepted 18th June 2018

DOI: 10.1039/c8ta03262a

rsc.li/materials-a

Realizing the best way to integrate electronics and textiles to develop smart wearable, functional apparel with multiple functionalities such as fibers with a unified capability to store and utilize energy is a significant topic of concern recently. Therefore, presenting a facile approach to obtain fibers with such unique properties in a continuous process is a forward contributing step towards the development of this field. Herein, a bottom-up approach to fabricate stretchable poly(styrene-butadiene-styrene)/few-layer graphene composite (SBS-G) fibers with unique organic vapor sensing behaviors and modified SBS-G fibers coated with electroactive carbon black (CB) nanofibers *via* modified electrospinning with excellent energy storage properties is presented. Unlike conventional conductive polymer composites (CPCs) that respond only to polar or non/low-polar organic vapors, the fabricated SBS-G composite fibers exhibited high sensitivity, excellent reversibility, and reproducibility as well as fast response to both polar and non/low-polar organic vapors. Moreover, the modified nanofiber-based SBS-G fibers demonstrated a high capacitive performance (78 F cm^{-3}), energy and power density (6.6 mW h cm^3 and 692 mW cm^3) and excellent flexibility. This study provides guidelines for the fabrication of ideal organic vapor sensors based on polymer composite fibers and an approach to modify any "off-the-shelf fiber" for fiber-based power storage.

Introduction

Traditional one-dimensional (1D) fibers (yarns) are the basic unit of textile fabrics which form different clothing sold to final consumers. With the emergence of smart wearable clothing and apparel, there has been continued increased focus to design functional fibers with unique properties, such as fibers with electroactive micro- to nano-diameters, reproducible surface-to-volume ratios, light weight, flexibility and conductivity with general suitability to be incorporated into traditional textiles with ease. Such functional fibers can find use in smart textiles as fiber supercapacitors,[8–11] batteries,[12,13] solar cells,[14,15] triboelectric nanogenerators,[16–18] sensors[19–22] and electrical conductors.[23]

Fiber-based sensors developed from conductive polymer composites (CPCs) should respond to external stimuli such as organic vapor, organic liquids, mechanical stress, biomolecules, humidity and temperature.[19,24–27] In particular, the fiber-based detection of volatile organic compounds (VOCs) is attracting tremendous research interest because many traditional organic gas-sensing devices reported so far employ bulky systems (*e.g.*, colorimetry and spectroscopy)[28,29] or require the incorporation of rigid electrodes (*e.g.*, interdigital electrodes) and substrates (*e.g.*, wafers, ceramics, and glass),[30,31] or in some cases need high operation temperatures (>200 °C)[32] which are not easy to integrate within textile wearable systems. In this line, recently, Kun *et al.*[33] reported a Metal–Organic Framework (MOF)-based wearable fiber with excellent detection of NO_2 even at 0.1 ppm without the requirement of high temperatures and could be flexed in different angles without performance failure. However, compared to conventional semiconducting metal oxides, carbon nanomaterials, and intrinsically conductive polymers, overall CPCs appear to be more suitable for fabricating organic vapor sensors because of their advantages, such as excellent chemical stability, hybrid nature, low operating temperatures, cost-effectiveness, tunable properties, wide

[a]State Key Laboratory for Modification of Chemical Fibers and Polymer Materials, College of Materials Science and Engineering, Donghua University, Shanghai 201620, P. R. China. E-mail: cmseysy@dhu.edu.cn; zhumf@dhu.edu.cn

[b]Research School of Engineering, College of Engineering and Computer Science, The Australian National University, Canberra, Australian Capital Territory 2601, Australia

[c]Leibniz Institute of Polymer Research Dresden, Hohe Straße 6, 01069 Dresden, Germany

[d]Centre for Nanofibers and Nanotechnology, National University of Singapore, 117581, Singapore

† Electronic supplementary information (ESI) available. See DOI: 10.1039/c8ta03262a

‡ Authors contributed equally towards this work.

application ranges and ease of fabrication.[34,35] The sensing principle of CPCs is based on the electrical resistance changes of composites in the presence of organic vapors. To be specific, organic vapor penetrates into the polymer that makes the polymer swell and then the conductive networks are re-arranged which results in the electrical resistance changes of the CPCs.

On the other hand, fiber supercapacitors and batteries are also commonly researched textile-based devices for powering various wearable electronics such as output displays for data obtained from such sensors described in the previous paragraph. In fact, various research groups have tried to report yarn-based energy storage devices with the required properties of high power and energy density.[8–11,36–39] However, the lingering challenge is to keep the high energy and power density values while introducing pure textile functions of stretchability and pliability with the ability to effortlessly weave and knit these energy yarns into fabrics and apparel. Furthermore, these devices should not fail or perform poorly when exposed to various unpredictable numerous textile bending positions during typical use.

With the above two functionalities in mind, a strategy to fabricate functional fibers with multiple applications such as being capable of acting as an organic vapor sensor and energy storage device would be utterly essential. Indeed, with material resources diminishing on the planet, recently, such approach is considered sustainable. Special functional fibers with organic vapor sensor and energy storage properties were reported in the recent past, for example, composites of MOFs/multiwalled carbon nanotubes (CNTs) with high sensitivity for hazardous gas monitoring and energy storage properties.[33] The fiber showed a very low detection limit for NO_2 down to almost 0.1 ppm and a high volumetric capacitance of 110 F cm^{-3}. However, despite the fascinating performance, developing such MOF-based fibers is quite a challenge due to the multiple steps involved to synthesize the materials employed. Therefore, if a facile and scalable approach together with traditional materials is employed and the synthesized materials still offer such competitive performances, they will be suitably better. And this formed the basis of the work in this report.

Typical electroactive materials of interest for supercapacitor electrodes commonly applied are transition metal oxides, conducting organic polymers and carbon materials. Transition metal oxides give raised specific capacitance values courtesy of their fast redox reactions but consequently downplayed by their intrinsic low electronic conductivities.[40–42] And conducting polymers can be tuned for excellent intrinsic conductivity (*via* doping) and offer relatively competitive specific capacitance (around 530 F g^{-1}) but poor cycle lifetime brought about by excessive expansion and contraction during the charge–discharge process.[43,44] However, carbon materials such as CNTs, graphene and carbon black (CB) are cheap and have a high surface area (up to 3000 m^2 g^{-1}), excellent electrical conductivity and chemical stability.[5,45] When such carbon materials are employed in CPCs, they offer the necessary performances. But to get the best out of them, it is necessary to form stable conductive networks with polymers having a high carbon loading. However, this impairs the mechanical properties and the processability of the composites.[19,20,46] Depending on the employed carbonaceous materials, the electrical percolation thresholds are different. For example, CNT filled CPCs require much lower loading than those of CB based CPCs due to the large aspect ratio and outstanding electrical conductivity of CNTs. Graphene, a two-dimensional monolayer of sp^2-hybridized carbon atoms in a honeycomb lattice has also attracted considerable attention for the fabrication of vapor sensors due to its remarkable properties such as a large sensing area, high electrical conductivity and thermal properties.[47,48] Another challenge with employing CPCs is that according to the sensing mechanism mentioned above, conventional CPC based vapor sensors respond only to vapors that have similar solubility parameters and polarities to their polymer matrix, which reduces the number of detectable vapors.[49,50] To overcome the problem of single side effectiveness, in this work poly(styrene-butadiene-styrene) (SBS), a kind of amorphous triblock copolymer, was selected as the polymer matrix of vapor sensors. According to 'like dissolves like' theory, SBS based CPC vapor sensors are expected to respond to both polar and non-polar solvent vapors due to the coexisting polar and non-polar segments in its molecular chain which can be swollen by polar

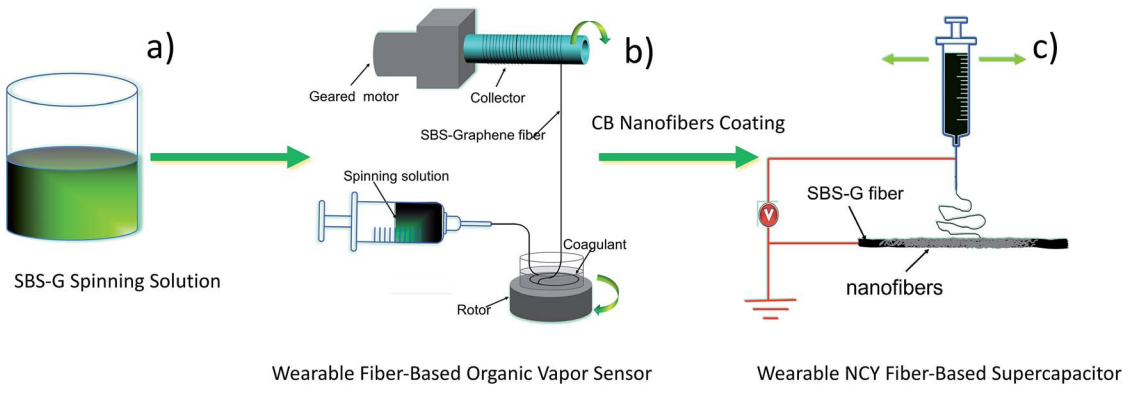

Scheme 1 A bottom-up approach to fabricate SBS-G composite fiber for fiber based organic vapor sensors, and further manipulation of the fiber for flexible energy storage applications which involved CB nanofiber self-assembly.

and non-polar vapors separately. This would lead to the reconstruction of the conductive network in the polymer matrix and hence a unique change in electrical resistance.

In this study, therefore, a bottom-up approach (Scheme 1) was employed which started with the fabrication of SBS-based composite fibers filled with different loading levels of few-layer graphene (FLG) *via* the wet spinning method. The resultant SBS-FLG composite fibers (SBS-G) were characterized as organic vapor sensors. The vapor sensing behavior of SBS-G composite fibers with different FLG contents was investigated by cyclic exposure to organic vapor and dry air in an alternating manner. The effects of the polarity of the organic vapor on the vapor sensing behaviors of the fiber were also evaluated using four kinds of organic vapors with different polarities. Then for energy storage properties, the SBS-G fibers were modified (with B nanofiber coating *via* templated electrospinning), and finally, their electrochemical performances were probed using standard electrochemical testing procedures of cyclic voltammetry (CV), galvanostatic charge–discharge (GCD), and electrochemical impedance spectroscopy (EIS). Overall, unlike many conventional conductive polymer composites that respond only to polar or non/low-polar organic vapors, the SBS-G composite fibers exhibited high sensitivity, excellent reversibility, and reproducibility as well as fast response to both polar and non/low-polar organic vapors. Moreover, the modified SBS-G composite fibers coated with CB nanofibers showed excellent electrochemical properties with a high energy density and power density of 6.6 mW h cm^3 and 692 mW cm^3, respectively.

Results and discussion

Organic vapor sensing behaviors of SBS-G fibers

First, the stretchable SBS-G fibers were fabricated through a facile and scalable wet-spinning process (for the detailed procedure see the Experimental section in the ESI and Fig. S1†). The samples are denoted as SBS-*x*G for simplification, where *x* represents the content of FLG in weight percentage. For instance, SBS-3G represents the composite fiber containing 3 wt% FLG.

The surface and cross-sectional morphologies of SBS-G composite fibers with different FLG loading are shown in Fig. 1

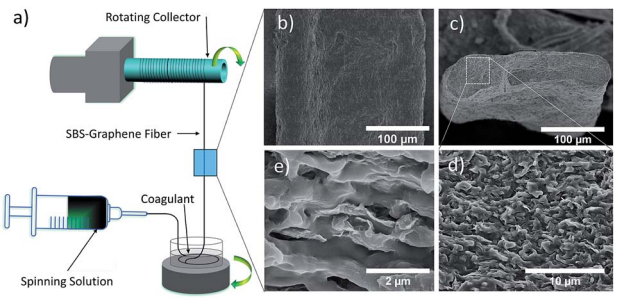

Fig. 1 SEM image analysis of SBS-G composite fiber. (a) Schematic for the fabrication of the SBS-G fiber. (b) SEM surface image of SBS-3G fiber and (c) cross-sectional image of SBS-3G fiber with its magnified images in (d) and (e).

and S2.† The surface images of the SBS-G composite fibers revealed a relatively rough morphology. All the SBS-G fibers generally appeared rough, which might benefit the quick adsorption and desorption of organic vapor which can translate to fast response and recovery times and in the same manner could be an excellent candidate for good electrochemical performances when employed as fiber electrodes in supercapacitors. The high-resolution cross-sectional SEM morphologies of SBS-3G fiber (Fig. 1d and e) showed that the FLG sheets were uniformly dispersed within the SBS matrix. The good interfacial adhesion between the SBS matrix and FLG sheets can also be confirmed in Fig. 1e, where the FLG sheets appeared well arranged within the SBS matrix.

Due to the presence of SBS, the composite fibers are expected to demonstrate excellent stretchability features. Therefore, these features were quantitatively analyzed by first stretching the fibers by 50% and then releasing them to their original length at a strain rate of 20 mm min^{-1} (then followed by 100%, 200% and 400% (Fig. S3†)). Within the plotted results in Fig. S3,† it can be observed that the elastic recovery sharply increases with applied low strains before eventually becoming linear (Fig. S3a†). And overall, for strains beyond 100%, elastic recovery decreased gradually with increased FLG loading. The strains in ranges above 100% qualify to label the fabricated SBS-G fibers stretchable, and this fulfils the critical stretch requirement in wearable yarns. The representative elastic recovery behavior of the SBS-3G fiber is also provided in Fig. S3b.†

The vapor sensing properties of SBS-G composite fibers were investigated by recording their resistance changes upon alternate exposure to (diluted) organic vapor. The VOC sensing behaviors of SBS-G composite fibers were investigated using four kinds of organic vapors with different polar solubility parameters (δ_P), including acetone (δ_P = 10.4 $MPa^{0.5}$), tetrahydrofuran (δ_P = 5.4 $MPa^{0.5}$), chloroform (δ_P = 3.1 $MPa^{0.5}$), and cyclohexane (δ_P = 0 $MPa^{0.5}$). A homemade dynamic measurement system (according to ref. 51) was employed which included mass flow controllers, solvent bubblers and a digital multimeter as illustrated in Fig. 2a (see the photographic image in Fig. S4†). Bubbling dry air in organic solvent provided a saturated vapor stream, which was in turn diluted with a second dry air flow to the desired concentration at 25 °C. The total flow rate was kept constant at 500 cm^3 min^{-1} by using two mass flow controllers (MFC 1 and MFC 2) during the measurements. The concentrations of the analytes (reported as percent (moles VOC)/(total moles of air)), which were carefully controlled by using the two MFCs, were calculated using eqn (1), where P is the input air pressure (which is atmospheric pressure in our system), and P_i (mmHg) is the saturated partial pressure of solvent empirically obtained by using the Antoine equation (eqn (2)), where A, B, and C are Antoine constants, and T is the temperature in Celsius. F and f are the mass flow rates of MFC 2 and MFC 1, respectively.

$$\text{Con } (\%) = \left[\frac{P_i}{P}\frac{f}{f+F}\right] \times 100 \quad (1)$$

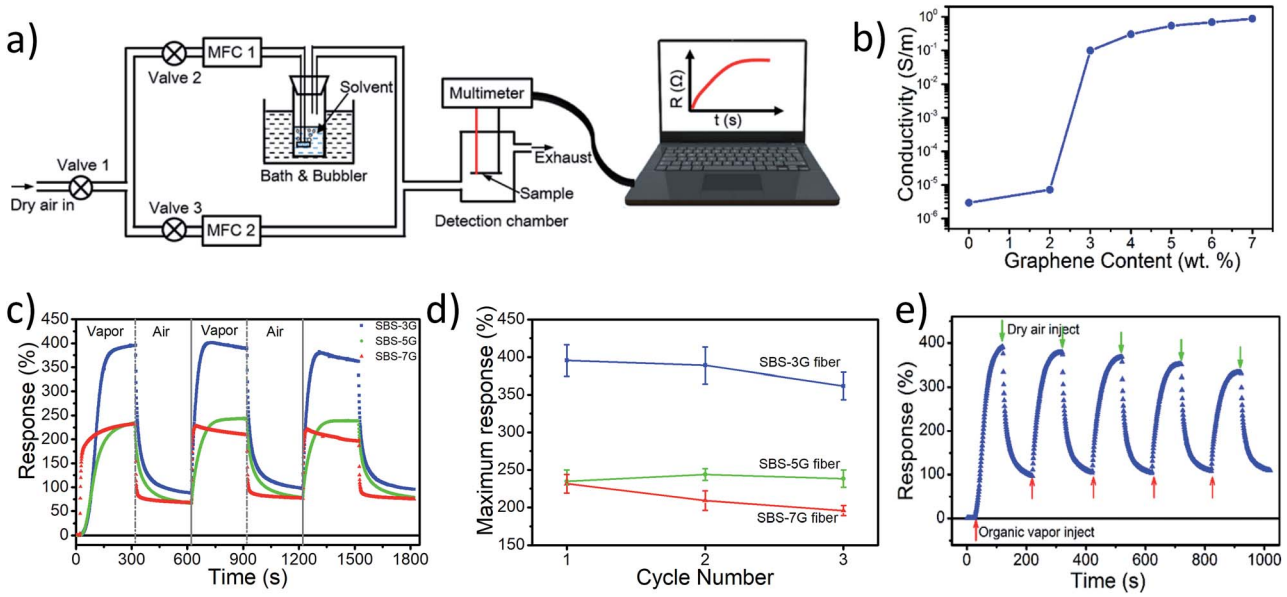

Fig. 2 (a) Schematic experimental setup for the detection of the vapor sensing behavior of SBS-G composite fibers for organic solvent vapors (see the photographic image in Fig. S4†), (b) conductivity of SBS-G composite fibers as a function of graphene content, (c) responsivity and (d) maximum responsivity of SBS-G composite fibers with different FLG contents upon cyclic exposure to 10% cyclohexane vapor at 25 °C. (e) Responsivity of SBS-3G composite fibers upon cyclic exposure to 10% cyclohexane vapor at 25 °C.

$$\lg P_i = A - \frac{B}{C + T} \quad (2)$$

The variation in electrical resistance was monitored online using a Keithley 2000 digital multimeter. The corresponding responsivity was calculated from the relative resistance change $((R - R_0)/R_0 \times 100\%$, where R_0 is the initial resistance of the sample in dry air and R is the real-time resistance measured during the experiment upon the alternating exposure to various analytes and dry air).

Fig. 2b shows the composite fiber conductivity *versus* FLG content, indicating that the conductivity of the SBS-G composite fiber increases with the FLG content. The electrical percolation of the SBS-G composite fiber was about 2.7 wt% and the conductivity increased from 10^{-6} S m^{-1} (pure SBS) to 10^{-1} S cm^{-1} (3 wt%). Then, the conductivity gradually increased to 1 S m^{-1} at 4 wt% FLG loading, and it almost levels off at a value of *ca.* 1 S m^{-1} at 7 wt% FLG loading.

It is expected and reported previously that the conductive filler content affects the sensitivity of CPC-based vapor sensors.[52] To understand the effect of different FLG contents, Fig. 2c shows the responsivity of SBS-G composite fibers with different FLG contents upon cyclic exposure to 10% cyclohexane vapor. The composite fibers with different FLG contents showed good reversibility and reproducibility. Fig. 2d illustrates that maximum responsivity decreased with the FLG loading during exposure to 10% cyclohexane vapor. This is due to the different FLG conductive network densities within the fibers, whereas the fibers containing low filler contents more near the electrical percolation threshold tend to show more pronounced destructions of FLG contacts during organic vapor adsorption and matrix swelling. It is worth noting that the SBS-7G fiber showed the fastest response and recovery. This can be attributed to the porous structure of the SBS-7G fiber, resulting in much faster procedures of VOC vapor adsorption and desorption on/from the composite fiber. However, to achieve both high and stable resistance responses, the samples with 3 wt% FLG loading (SBS-3G) were selected for further investigations.

One of the critical parameters in organic vapor sensing studies is the response time. This is defined as the time taken by the sensor to acquire 90% of the maximum resistance in the presence of analyte vapor. The response times of SBS-3G fibers upon exposure to different VOC vapors are shown in Fig. S5.† In general, the response time was less than 46 s upon exposure to 10% VOC vapors, which is much shorter than the results reported in previous literature.[53–55] This is ascribed to the micrometer diameters, high surface areas and non-uniform surfaces of the fibers, which all enabled good adsorption and permeation of VOC vapor into the specimen fibers.

Fig. 2e shows the responsivity of SBS-3G composite fibers during exposure to cyclohexane (Con. = 10%) vapor pulse. Before exposure to the target analyte, the resistance was recorded for 20 s under dry air to get a stable initial resistance value. Then, SBS-3G composite fiber was exposed to cycles of alternating gas pulses of diluted cyclohexane vapor and dry air. When the composite fibers were exposed to organic solvent vapor, it was found that the resistance increased quickly as expected. In addition, the SBS-3G fiber conductivity was also able to quickly decrease as the fiber was exposed to dry air. All this indicates that the resistance changes of SBS-3G composite fiber upon exposure to cyclohexane vapor exhibited fast and reproducible responsiveness. The resistance response curve shows 100% hysteresis to the initial resistance value in the first cycle

due to the re-arrangement of the conductive network. However, the maximum responsivity decreased slightly with each cycle due to the retention of some cyclohexane molecules adsorbed by SBS-3G composite fibers during the desorption procedure, making some FLG slightly separated from the SBS matrix.[34]

Any vapor sensor should be able to respond to relatively low concentrations of vapor for reliability especially during usage in the case of leakages. In this line, therefore, the sensing behaviors of SBS-3G fibers upon exposure to different concentrations of cyclohexane vapor (Fig. S6†) were determined. Generally, the response rate of the fibers increased with rising vapor concentration. Similar results were reported in many previous studies.[19,56]

In addition to cyclohexane, other organic solvent vapors with various polar solubility parameters (δ_P) (Table 1) were used to evaluate the responsivity of SBS-3G fiber. As illustrated in Fig. 3a, the SBS-3G fiber showed good reversibility and reproducibility upon exposure to both polar and non/low-polar organic vapors. Overall, the fiber exhibited relatively high sensitivity to both polar and non/low-polar organic vapors, demonstrating its wide detection range, which is preponderant among other recently reported vapor sensors.[53,54,57] The maximum responsivity of the composite fiber to different VOCs decreased with the rising δ_P of the solvents, Fig. 3b. This is attributed to the diverse interactions between the solvent molecules and the SBS matrix. It is known that SBS is a segmented polymer consisting of long no-polar soft segments and short polar hard segments that constitute a unique microphase separation structure. According to the rule of "like dissolves like",[58] the non-polar soft segments (polybutadiene domains) of SBS can be swollen by low-and non-polar solvents. Similarly, the hard-polar segments (polystyrene domains) can be dissolved in polar solvents and hence lead to volume expansion of the matrix. Nevertheless, owing to the fact that the swelling degree of SBS upon exposure to high polar solvent vapors is much less than that observed upon exposure to low/non-polar solvent vapors, the responses of SBS-G composite fibers to non/low-polar solvent vapors are much higher than that to polar solvent vapors.

In the process of practical applications, the vapor sensor may be exposed to mixed organic vapors. Therefore, the influence of three different mixed vapors on the sensing performance of SBS-3G fiber was demonstrated. As shown in Fig. 3c, the SBS-3G fiber showed good reversibility and reproducibility upon exposure to different mixtures. The ranking of maximum responsivity to mixed organic vapor with different δ_P is as follows: 5% cyclohexane and 5% tetrahydrofuran > 5% cyclohexane and 5% acetone > 5% tetrahydrofuran and 5% acetone. The sensitivity of SBS-3G fiber to the mixture is in accordance with that of single organic vapor. This finding could be explained by the rule of "like dissolves like" as mentioned earlier.

The mechanical reliability of SBS-3G fiber was also determined according to the experiments designed in our previous work with the help of a homemade two-point bending device.[19] During that time, the relative resistance changes of the SBS-3G composite fiber without bending and after 1000 bending–straightening cycles upon cyclic exposures to 10% cyclohexane vapor were obtained (Fig. S7†). The fiber after these various bending–straightening cycles showed almost the same response as that of the fiber without bending. The results signify that the fabricated SBS-3G composite fibers have reliable and excellent mechanical flexibility fitting for use as fibre-based sensors. Consequently, this means that the fibers can efficiently be woven into textiles *via* knitting or weaving and retain their testing (laboratory) vapor sensing capabilities prior to use by the final consumer in wearable smart textiles.

Modification of SBS-G composite yarn for energy storage applications

Functional fiber materials obtained with ease and with known fabrication techniques such as facile wet spinning and traditional electrospinning with more than one function are desirable for future smart textiles owing to the ease and scalability of the approaches.[60,61] When such fibers are incorporated into functional wearable clothing, they offer the functional ability of a wide range of applications and have potential to lower the overall material costs. After a proven demonstration of the SBS-G fiber to work as an organic vapor sensor, we proceeded to find out if it could also work as a fiber electrode for energy storage in yarn supercapacitors or batteries.

In the first part of these experiments, the SBS-7G fiber was considered as a fiber electrode due to its better conductivity (compared to other samples) attributed to the increased FLG loading in the SBS polymer (see Fig. 2b). The fibers were assembled into fiber-based devices with the help of the PVA/H_2SO_4 gel electrolyte as described in S1.1 of the ESI.† The assembled devices were then standard tested with CV, GCD, and EIS electrochemical tests. However, the performance of the SBS-7G was lacking which called for further fiber modification for better electrochemical behaviors. One of the most commonly used textile fiber modification is a coating of active materials

Table 1 Characteristics of solvents used for vapor sensing experiments[59]

Solvent	δ^a [$MPa^{0.5}$]	$\delta_D{}^b$ [$MPa^{0.5}$]	$\delta_P{}^c$ [$MPa^{0.5}$]	$\delta_H{}^d$ [$MPa^{0.5}$]	V_{mol} [$cm^3\ mol^{-1}$]
Acetone	19.9	15.5	10.4	7.0	73.52
Tetrahydrofuran	19.5	16.8	5.7	8.0	81.02
Chloroform	18.9	17.8	3.1	5.7	80.66
Cyclohexane	16.8	16.8	0.0	0.0	130.58

[a] Global Hansen solubility parameter $(MPa)^{1/2}$. [b] Dispersive component of the Hansen solubility parameter $(MPa)^{1/2}$. [c] Polar component of the Hansen solubility parameter $(MPa)^{1/2}$. [d] Hydrogen bonding component of the Hansen solubility parameter $(MPa)^{1/2}$.

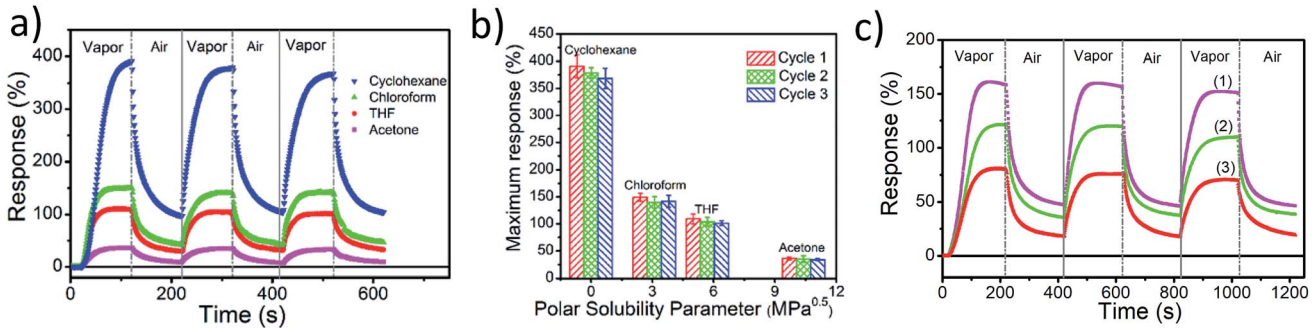

Fig. 3 (a) Responsivity of SBS-3G composite fibers upon exposure to various solvent vapors (Con. = 10%); (b) maximum responsivity of SBS-3G composite fibers upon exposure to various solvent vapors (Con. = 10%) during the first three exposure cycles *versus* the polar component of the Hansen solubility parameter; (c) responsivity of SBS-3G composite fibers towards mixed solvent vapors: (1) 5% cyclohexane and 5% tetrahydrofuran; (2) 5% cyclohexane and 5% acetone; (3) 5% tetrahydrofuran and 5% acetone.

such as carbon-based materials or conducting polymers for electrochemical improvements, the reason being that the coatings tend to provide a continuous conducting layer.[11] It is worth noting that coating methods present a couple of disadvantages. More critically, coating fibers with active materials significantly diminishes the fibers' surface area and flexibility. Also, the active materials on the coated fibers are susceptible to cracking/peeling when the fibers are held or used in non-straight positions. With this reasoning, in the recent past, our group proposed the nanofiber coated yarn concept as a solution to problems in coated fibers.[11] Following the lessons learnt previously, we employed Super-P CB as a coating to boost the electrochemical performance of the SBS-7G fiber. Balanced electrochemical comparisons were drawn between modified SBS-7G fiber slurry coated with CB spinning solution (SBS-7G@CB) (Fig. S8†) and nanofibers coated with CB electrospun nanofibers (SBS-7G NCY) (Fig. 4) (for preparation details of the SBS-7G@CB and SBS-7G NCY samples see the Experimental section in the ESI†).

First, SEM image analysis was done as provided in Fig. S8† and 4 for SBS-7G@CB and SBS-7G NCY, respectively. We can observe a big difference between the slurry-based coating and nanofiber-based coating employed to modify the SBS-7G. Although both coatings were uniform, the nanofiber coating presented quite a unique and networked nanofiber morphology. Beyond presenting such unique coating architectures, the process of electrospinning nanofibers on SBS-7G fiber is scalable and controllable[11] with a great ability to give resultant functional yarns with flexibility maintained. This relies on the fact that coatings tend to crack easily during fiber flexing in use or even during incorporation into apparel, for example during textile manufacturing such as weaving and knitting. Therefore, in this sense, the SBS-7G NCY presents many advantages over the SBS-7G@CB. Also, such surface morphologies are predicted to offer great electrochemical performance when employed as electrodes,[43,62,63] and this was probed and substantiated in the next part of the article.

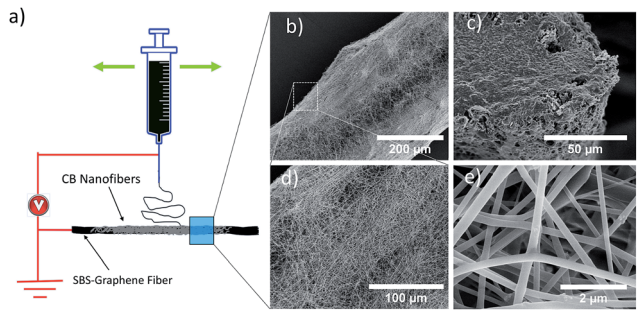

Fig. 4 SEM image analysis of SBS-7G NCY. (a) Schematic for the self-assembly of CB nanofibers on the SBS-7G fiber. (b) SEM surface image of SBS-7G NCY with its magnified images in (d) and (e) and (c) cross-sectional image of SBS-7G NCY.

Symmetric electrochemical fiber devices were prepared using either SBS-7G, SBS-7G@CB or SBS-7G NCY as an electrode. Two such electrodes were arranged parallel with the PVA/H_2S0_4 gel electrolyte (for electrolyte preparation see the ESI S1.1†). CV and GCD curves for the devices made with SBS-5G, SBS-7G@CB and SBS-7G NCY yarn electrodes are compared in Fig. 5a and b, respectively (see others in Fig. S9 and S10†). All devices showed quasi-rectangular CV curves and triangular GCD curves attributed to the electrochemical double-layer charging capacitance of the carbonaceous materials such as the used graphene and CB.[64] From the CV curves, it can be observed that nanofiber-modified SBS-7G NCY had more area followed by slurry-modified SBS-7G@CB as compared to the neat SBS-7G device. To be specific, at 5 mV s^{-1} the calculated device specific capacitance was as high as 270 F g^{-1} (60.2 F cm^{-3} and 300 mF cm^{-2}), 246 F g^{-1} (54.4 F cm^{-3} and 240 mF cm^{-2}), and 166 F g^{-1} (36.9 F cm^{-3} and 200 mF cm^{-2}) for SBS-7G NCY, SBS-7G@CB and SBS-5G devices, respectively. A similar performance trend can also be observed with GCD tests (1.0 A g^{-1}) presented in Fig. 5b, where the gravimetric capacitance was 303.3 F g^{-1}, 250 F g^{-1} and 172 F g^{-1} for SBS-7G NCY, SBS-7G@CB and SBS-5G devices, respectively. The best performance of the SBS-7G NCY is much attributed to the electroactive nanofibrous and porous layer of CB nanofibers on the SBS-7G fiber.[65] Unlike the SBS-7G@CB, the CB electrospun nanofiber coating on SBS-7G NCY electrodes is capable of offering unique nanostructured architectures with improved electrochemical performance.[11,43,61]

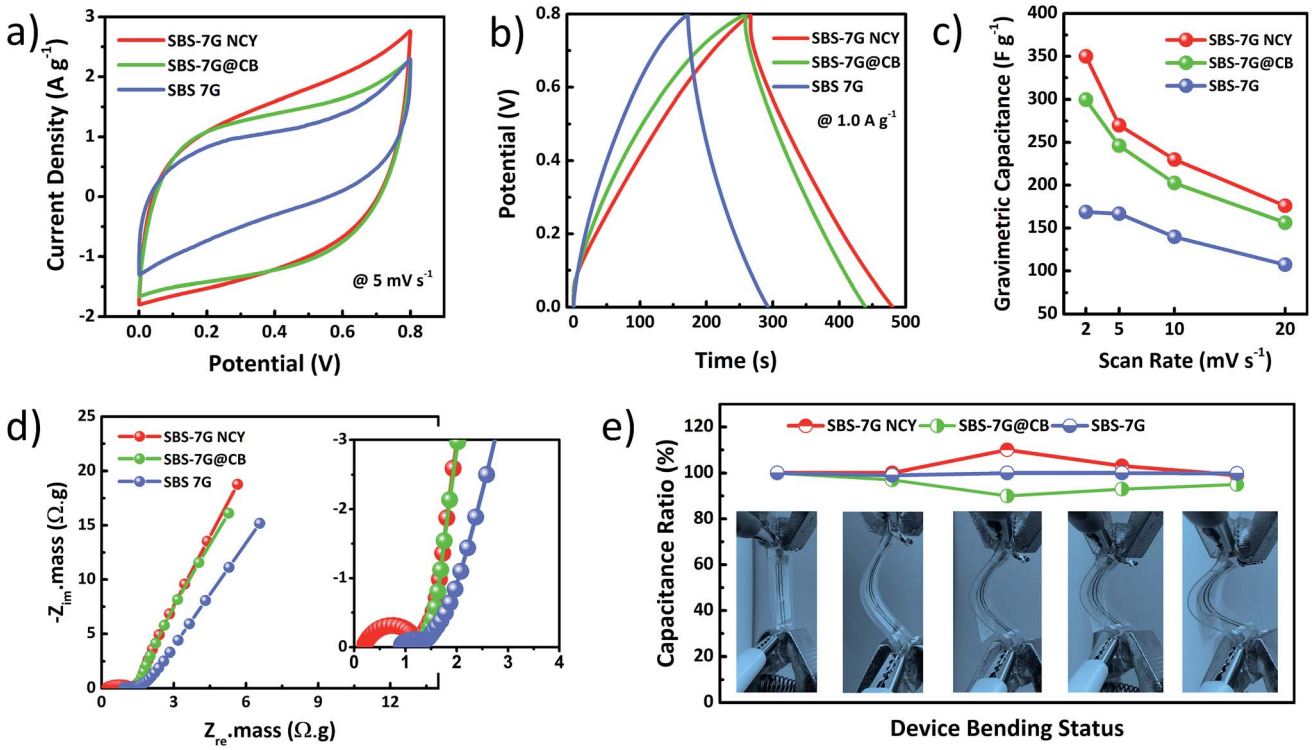

Fig. 5 Electrochemical comparison tests of SBS-7G, SBS-7G@CB, and SBS-7G NCY. (a) CV curves of the fibers at a scan rate of 5 mV s^{-1}, (b) GCD curves at a current density of 1.0 A g^{-1}, (c) variation of the fiber gravimetric capacitance with the scan rate, (d) EIS plots with their high-frequency regions in the inset (side) and (e) capacitance ratio in percentage (C/C_0, where C_0 is the initial capacitance) under different bending conditions at a scan rate of 20 mV s^{-1}.

Such a morphology is known to offer an efficient electron and ion diffusion which apparently translates to improved values of capacitance.[43,66] The highest values of volumetric (areal) capacitances determined at 2 mV s^{-1} were 78 F cm^{-3} (390 mF cm^{-2}), 66.2 F cm^{-3} (360 mF cm^{-2}) and 37.3 F cm^{-3} (197 mF cm^{-2}) for SBS-7G NCY, SBS-7G@CB and SBS-5G devices, respectively. This signifies that the facile modification technique of NCY concept employed is relevant and universally applicable.

The scan rate retention of the assembled devices was also probed. Fig. 5c shows the variation of SBS-7G NCY, SBS-7G@CB and SBS-5G device specific capacitance with different scan rates (2, 5, 10, and 20 mV s^{-1}). Generally, the capacitance decreased with increasing scan rate. To be specific SBS-7G NCY, SBS-7G@CB and SBS-5G showed a good rate retention of 50.3%, 52.1% and 63.5%, respectively (2–20 mV s^{-1}). It should be noted that the modified fiber devices showed a greater percentage capacitance loss with changing scan rates than the neat SBS-7G. However, despite such observations, still, the capacitance of the SBS-7G NCY device was competitive at a 20 mV s^{-1} scan rate to a tune of 176.1 F g^{-1} (39.2 F cm^{-3} and 200 mF cm^{-2}). EIS tests were also considered to determine the electrochemical properties of fibers in the assembled devices. From the results in Fig. 5d, the Z_{re} mass values of the devices were in the order of SBS-5G > SBS-7G@CB > SBS-7G NCY. The shift of the SBS-5G value to the right is due to its poor conductivity. And, the plots for the modified SBS-7G NCY and SBS-7G@CB composite fibers showed better performance being nearly vertical to the Z_{im} axis due to better ion movement within the electrodes. Moreover, the plot of SBS-7G NCY shifted more to the left, implying that such nanofiber modified fiber could provide better nanofibrous channels for quick ion diffusion.[5,67] Bending tests were performed to determine the flexibility performance of the fiber-based devices for possible applications in wearable energy storage systems. Due to their single dimensions, the electrochemical performances could be well maintained under various deformations (Fig. 5e) with a notable loss of capacitance in SBS-7G@CB. Such an observation is attributed to the coated active material problems previously discussed which tend to crack off with ease during bending and hence fall in capacitance[11] The observations make nanofiber coated fibers more preferable than slurry coated fibers due to their resilience and flexibility, especially in wearable smart textiles and electronics.

From the preliminary tests in Fig. 5, it can be seen that the modified SBS-7G NCY device showed the best performance which is attributed to the electroactive nanostructured fibrous surface and the presence of conductive CB.[68] Therefore, further electrochemical probing was done on the SBS-7G NCY device wherein the device was cycled from 2 to 50 mV s^{-1} as shown in Fig. 6a for CV tests and also GCD tests were performed within a range of current densities from 0.5–5.0 A g^{-1} (Fig. 6b). Large area CV curves indicating good device performance can be observed. The specific capacitance values obtained across the tested scan rates ranged from 350 F g^{-1} (78 F cm^{-3} and 390 mF

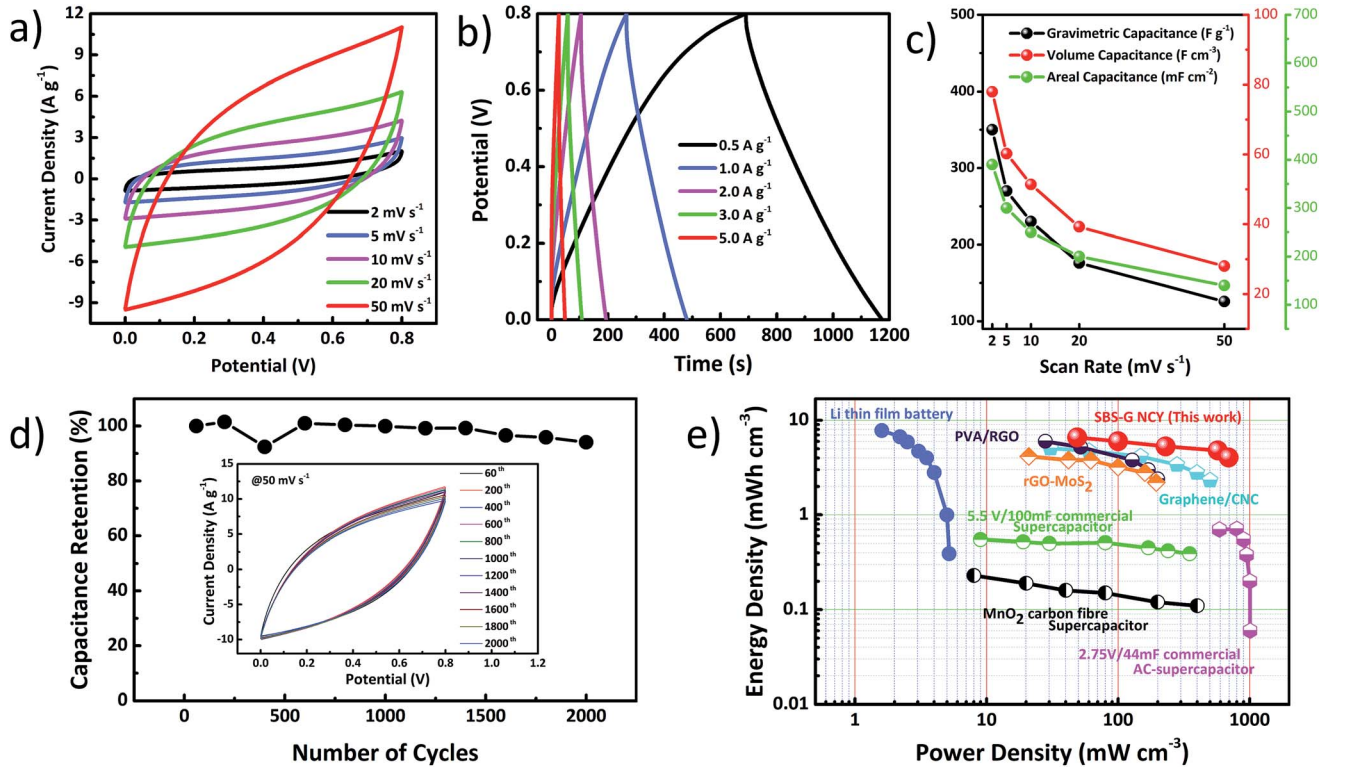

Fig. 6 Electrochemical performance of the SBS-7G NCY device. (a) CV and (b) GCD curves at various scan rates and current densities, respectively, (c) variation of specific capacitance values with the scan rate obtained from the CV curves in (a), (d) capacitance retention ability over 2000 cycles at a scan rate of 50 mV s^{-1} (inset), and (e) the Ragone plot of the device in comparison to other state-of-the-art devices in the literature.[1–7]

cm^{-2}) to 125.8 F g^{-1} (28 F cm^{-3} and 140 mF cm^{-2}) from 2 to 50 mV s^{-1}. These values of capacitance are better than those of many previously reported fiber-based devices in the literature, such as reduced graphene oxide (RGO)/alginate calcium–PVA/RGO direct spun supercapacitors (35 mF cm^{-2}),[69] fiber supercapacitors made of RGO active materials (1.2 mF cm^{-2} to 3.33 mF cm^{-2}),[70,71] CNT-based fiber supercapacitors (8.66 mF cm^{-2} and 40.9 mF cm^{-2}),[72,73] conducting polymer polyindole/CB NCY (16.44 mF cm^{-2})[11] and commercial pen ink supercapacitors (19.5 mF cm^{-2}).[74] Also, the specific capacitance values of the SBS-7G NCY device were maintained at 77.1%, 65.9%, and 50.3%, 36% at scan rates of 5, 10, 20, and 50 mV s^{-1}, respectively with respect to the capacitance obtained at 2 mV s^{-1} (Fig. 6c), signifying good rate capability of the modified fiber device.

Capacitance cycle retention in energy storage devices is another primary quality required. Therefore, to understand the capacitance cycle retention ability of the modified SBS-7G NCY, the fiber device was cycled at 50 mV s^{-1} in a standard CV test method (Fig. 6d). The specific capacitance was calculated only to be retained to a tune of 94% after 2000 cycles indicating excellent cycle stability. Previously, such excellent cycle retention performance has been attributed to polymer-based nanofiber composites capable of presenting a dense morphology coating capable of withstanding an unlimited bulge caused by continuous charge–discharge currents within the fiber electrodes.[66] These values of retention are better than those of the fiber devices previously reported in our studies for graphene/cellulose nanocrystal fibers (92.1% (1000 cycles)),[5] non-liquid-crystal spun graphene fibers (92% (1000 cycles)),[60] and PVA/graphene fibers (85% (1000 cycles)).[45] Energy density and power density are also crucial factors which when plotted on a Ragone plot can provide a bird's view of the performance of any energy storage device in comparison with others.[75] Fig. 6e gives a summarized Ragone plot of the SBS-7G NCY device in comparison with others in the literature showing a maximum energy density of up to 6.6 mW h cm^{-3} and power density of 49 mW cm^{-3} at a current density of 0.5 A g^{-1} (Table S1†). This energy density value is superior but comparable to those of our previously reported fiber based supercapacitors of graphene/CNC fiber (5.1 mW h cm^{-3} at 30.7 mW cm^{-3}),[5] PVA/RGO hybrid fiber-based supercapacitors (5.97 mW h cm^{-3})[45] and hierarchical MnO_2/RGO fiber-based devices.[76] It is worth noting that the energy density values of the SBS-7G NCY device was also better than those of commercially available supercapacitors (2.75 V/44 mF and 5.5 V/100 mF),[6,7] RGO–MoS_2 fiber supercapacitors (4.15 mW h cm^{-3} at 21 mW cm^{-3}),[2] and MnO_2/carbon fiber supercapacitors (0.23 mW h cm^{-3} at 8 mW cm^{-3}),[4] and even reasonably comparable with that of Li-thin film batteries.[3] Moreover, The maximum power density of the reported device was 692.6 mW cm^{-3}, which value is placed relatively close to that of commercially available supercapacitors

and quite superior by almost two orders of magnitude to that of lithium thin-film batteries.[3,6] The electrochemical results and discussions demonstrated that the facilely fabricated stretchable SBS-G modified by CB nanofiber coating *via* a traditional and scalable NCY technique exhibited excellent electrochemical properties fitting for use in wearable energy storage applications too.

Conclusions

SBS-G composite fibers were successfully prepared *via* the wet spinning method. When the fibers were exposed to organic vapors, their electrical resistance significantly changed, which could be rapidly recovered latter as the specimens were transferred to dry air. It is thus demonstrated that the composites are suitable to be used as vapor sensors. The vapor responsivity depended on the FLG content and the δ_P value of the organic solvents. Lower FLG loadings (3 wt%) resulted in larger responsivity (*ca.* 400%) upon exposure to 10% cyclohexane. Compared with a conventional CPC based vapor sensor that exhibited limited applicability, the SBS-G composite fibers were capable of responding to a wide range of solvents including low/non-polar and polar solvent vapors due to the coexistence of non-polar and polar segments on SBS chains. More still, the SBS-3G fiber showed good reversibility and reproducibility upon exposure to mixtures of organic vapor with different δ_P. Moreover, when SBS-7G fiber was modified *via* coating of CB nanofibers using modified electrospinning coating, the resultant fiber showed excellent electrochemical performance with superior flexibility as compared to the slurry-based coated fiber (SBS-7G@CB) and unmodified SBS-G fiber owing to the nanostructured surface and fibrous morphology which presents unobstructed nano-channels ideal for ion movement during electrochemical performance. The performance values of the SBS-7G NCY fiber-based device were as high as 78 F cm^{-3} (350 F g^{-1} and 390 mF cm^{-3}) at 2 mV s^{-1}, and it showed excellent cycling stability (94% capacitance retention after 2000 cycles) and high energy density and power density (6.6 mW h cm^3 and 692 mW cm^3), respectively. This work details a facile continuous approach to fabricate 1D multi-functional-based fiber materials using two commonly used techniques of wet spinning and electrospinning utilizing each technique's strength in quite a systematic manner. It is worth noting that the technique of coating nanofibers *via* modified electrospinning onto the fibers is universal as it can be extended even to "off-the-shelf" fibers/yarns.

Conflicts of interest

There are no conflicts to declare.

Acknowledgements

The authors are very much grateful for the funds from the Science and Technology Commission of Shanghai Municipality (16JC1400700), the National Key Research and Development Program of China (2016YFA0201702/2016YFA0201700), the "Chenguang Program" supported by the Shanghai Education Development Foundation, the Shanghai Municipal Education Commission (15CG32), the National Natural Science Foundation of China (Grant No. 51673088), the Fundamental Research Funds for the Central Universities, the DHU Distinguished Young Professor Program, the Program for Innovative Research Team in University of Ministry of Education of China (IRT_16R13), and the Program of Introducing Talents of Discipline to Universities (No. 111-2-04).

Notes and references

1 Y. Yu, Y. Sun, C. Cao, S. Yang, H. Liu, P. Li, P. Huang and W. Song, *J. Mater. Chem. A*, 2014, **2**, 7706–7710.
2 G. Sun, J. Liu, X. Zhang, X. Wang, H. Li, Y. Yu, W. Huang, H. Zhang and P. Chen, *Angew. Chem., Int. Ed.*, 2014, **53**, 12576–12580.
3 D. Pech, M. Brunet, H. Durou, P. Huang, V. Mochalin, Y. Gogotsi, P.-L. Taberna and P. Simon, *Nat. Nanotechnol.*, 2010, **5**, 651.
4 X. Xiao, T. Li, P. Yang, Y. Gao, H. Jin, W. Ni, W. Zhan, X. Zhang, Y. Cao, J. Zhong, L. Gong, W.-C. Yen, W. Mai, J. Chen, K. Huo, Y.-L. Chueh, Z. L. Wang and J. Zhou, *ACS Nano*, 2012, **6**, 9200–9206.
5 G. Chen, T. Chen, K. Hou, W. Ma, M. Tebyetekerwa, Y. Cheng, W. Weng and M. Zhu, *Carbon*, 2018, **127**, 218–227.
6 M. F. El-Kady, V. Strong, S. Dubin and R. B. Kaner, *Science*, 2012, **335**, 1326–1330.
7 M. F. El-Kady and R. B. Kaner, *Nat. Commun.*, 2013, **4**, 1475.
8 D. Yu, Q. Qian, L. Wei, W. Jiang, K. Goh, J. Wei, J. Zhang and Y. Chen, *Chem. Soc. Rev.*, 2015, **44**, 647–662.
9 F. Meng, Q. Li and L. Zheng, *Energy Storage Mater.*, 2017, **8**, 85–109.
10 W. Ma, S. Chen, S. Yang, W. Chen, W. Weng, Y. Cheng and M. Zhu, *Carbon*, 2017, **113**, 151–158.
11 M. Tebyetekerwa, Z. Xu, W. Li, X. Wang, I. Marriam, S. Peng, S. Ramkrishna, S. Yang and M. Zhu, *ACS Appl. Energy Mater.*, 2018, **1**, 377–386.
12 Y. Zhang, Y. Zhao, J. Ren, W. Weng and H. Peng, *Adv. Mater.*, 2016, **28**, 4524–4531.
13 Y.-H. Lee, J.-S. Kim, J. Noh, I. Lee, H. J. Kim, S. Choi, J. Seo, S. Jeon, T.-S. Kim, J.-Y. Lee and J. W. Choi, *Nano Lett.*, 2013, **13**, 5753–5761.
14 Z. Yang, J. Deng, X. Sun, H. Li and H. Peng, *Adv. Mater.*, 2014, **26**, 2643–2647.
15 R. Li, X. Xiang, X. Tong, J. Zou and Q. Li, *Adv. Mater.*, 2015, **27**, 3831–3835.
16 Y. Yang, N. Sun, Z. Wen, P. Cheng, H. Zheng, H. Shao, Y. Xia, C. Chen, H. Lan, X. Xie, C. Zhou, J. Zhong, X. Sun and S.-T. Lee, *ACS Nano*, 2018, **12**, 2027–2034.
17 M. Zhang, T. Gao, J. Wang, J. Liao, Y. Qiu, Q. Yang, H. Xue, Z. Shi, Y. Zhao, Z. Xiong and L. Chen, *Nano Energy*, 2015, **13**, 298–305.
18 K. N. Kim, J. Chun, J. W. Kim, K. Y. Lee, J.-U. Park, S.-W. Kim, Z. L. Wang and J. M. Baik, *ACS Nano*, 2015, **9**, 6394–6400.
19 X. Wang, Y. Li, J. Pionteck, Z. Zhou, W. Weng, X. Luo, Z. Qin, B. Voit and M. Zhu, *Sens. Actuators, B*, 2018, **256**, 896–904.

20 X. Wang, S. Meng, M. Tebyetekerwa, Y. Li, J. Pionteck, B. Sun, Z. Qin and M. Zhu, *Composites, Part A*, 2018, **105**, 291–299.
21 Z. Liu, D. Qi, G. Hu, H. Wang, Y. Jiang, G. Chen, Y. Luo, X. J. Loh, B. Liedberg and X. Chen, *Adv. Mater.*, 2018, **30**, 1704229.
22 J. Zhang, Y. Cao, M. Qiao, L. Ai, K. Sun, Q. Mi, S. Zang, Y. Zuo, X. Yuan and Q. Wang, *Sens. Actuators, A*, 2018, **274**, 132–140.
23 Z. F. Liu, S. Fang, F. A. Moura, J. N. Ding, N. Jiang, J. Di, M. Zhang, X. Lepró, D. S. Galvão, C. S. Haines, N. Y. Yuan, S. G. Yin, D. W. Lee, R. Wang, H. Y. Wang, W. Lv, C. Dong, R. C. Zhang, M. J. Chen, Q. Yin, Y. T. Chong, R. Zhang, X. Wang, M. D. Lima, R. Ovalle-Robles, D. Qian, H. Lu and R. H. Baughman, *Science*, 2015, **349**, 400.
24 J. Lee, H. Kwon, J. Seo, S. Shin, J. H. Koo, C. Pang, S. Son, J. H. Kim, Y. H. Jang, D. E. Kim and T. Lee, *Adv. Mater.*, 2015, **27**, 2433–2439.
25 Q. F. Ma, Z. Q. Tou, K. Ni, Y. Y. Lim, Y. F. Lin, Y. R. Wang, M. H. Zhou, F. F. Shi, L. Niu, X. Y. Dong and C. C. Chan, *Sens. Actuators, B*, 2018, **257**, 800–806.
26 Z. Gao, Z. Lou, S. Chen, L. Li, K. Jiang, Z. Fu, W. Han and G. Shen, *Nano Res.*, 2018, **11**, 511–519.
27 M. Bariya, H. Y. Y. Nyein and A. Javey, *Nature Electronics*, 2018, **1**, 160–171.
28 L. Feng, C. J. Musto and K. S. Suslick, *J. Am. Chem. Soc.*, 2010, **132**, 4046–4047.
29 Y. Li, S. Zhang and D. Song, *Angew. Chem.*, 2013, **125**, 738–741.
30 S. Cui, H. Pu, S. A. Wells, Z. Wen, S. Mao, J. Chang, M. C. Hersam and J. Chen, *Nat. Commun.*, 2015, **6**, 8632.
31 O. Yassine, O. Shekhah, A. H. Assen, Y. Belmabkhout, K. N. Salama and M. Eddaoudi, *Angew. Chem., Int. Ed.*, 2016, **55**, 15879–15883.
32 Y. Bae, P. V. Pikhitsa, H. Cho and M. Choi, *Adv. Mater.*, 2017, **29**, 1604159.
33 K. Rui, X. Wang, M. Du, Y. Zhang, Q. Wang, Z. Ma, Q. Zhang, D. Li, X. Huang, G. Sun, J. Zhu and W. Huang, *ACS Appl. Mater. Interfaces*, 2018, **10**, 2837–2842.
34 Q. Fan, Z. Qin, T. Villmow, J. Pionteck, P. Pötschke, Y. Wu, B. Voit and M. Zhu, *Sens. Actuators, B*, 2011, **156**, 63–70.
35 J. F. Feller, J. Lu, K. Zhang, B. Kumar, M. Castro, N. Gatt and H. J. Choi, *J. Mater. Chem.*, 2011, **21**, 4142–4149.
36 W. Weng, P. Chen, S. He, X. Sun and H. Peng, *Angew. Chem., Int. Ed.*, 2016, **55**, 6140–6169.
37 W. Zeng, L. Shu, Q. Li, S. Chen, F. Wang and X.-M. Tao, *Adv. Mater.*, 2014, **26**, 5310–5336.
38 X. Wang, K. Jiang and G. Shen, *Mater. Today*, 2015, **18**, 265–272.
39 Q. Huang, D. Wang and Z. Zheng, *Adv. Energy Mater.*, 2016, **6**, 1600783.
40 Z. Wu, Y. Zhu and X. Ji, *J. Mater. Chem. A*, 2014, **2**, 14759–14772.
41 Y. Liu, Z. Wang, Y. Zhong, M. Tade, W. Zhou and Z. Shao, *Adv. Funct. Mater.*, 2017, **27**, 1701229.
42 Y. Liu, Z. Wang, M. Veder Jean-Pierre, Z. Xu, Y. Zhong, W. Zhou, O. Tade Moses, S. Wang and Z. Shao, *Adv. Energy Mater.*, 2018, **8**, 1702604.
43 M. Tebyetekerwa, S. Yang, S. Peng, Z. Xu, W. Shao, D. Pan, S. Ramakrishna and M. Zhu, *Electrochim. Acta*, 2017, **247**, 400–409.
44 A. M. Bryan, L. M. Santino, Y. Lu, S. Acharya and J. M. D'Arcy, *Chem. Mater.*, 2016, **28**, 5989–5998.
45 S. Chen, W. Ma, H. Xiang, Y. Cheng, S. Yang, W. Weng and M. Zhu, *J. Power Sources*, 2016, **319**, 271–280.
46 P. Costa, C. Silvia, J. C. Viana and S. Lanceros Mendez, *Composites, Part B*, 2014, **57**, 242–249.
47 C. Soldano, A. Mahmood and E. Dujardin, *Carbon*, 2010, **48**, 2127–2150.
48 H. Liu, W. Huang, X. Yang, K. Dai, G. Zheng, C. Liu, C. Shen, X. Yan, J. Guo and Z. Guo, *J. Mater. Chem. C*, 2016, **4**, 4459–4469.
49 J. Lu, B. Kumar, M. Castro and J.-F. Feller, *Sens. Actuators, B*, 2009, **140**, 451–460.
50 M. Castro, J. Lu, S. Bruzaud, B. Kumar and J.-F. Feller, *Carbon*, 2009, **47**, 1930–1942.
51 Y. S. Kim, S.-C. Ha, H. Yang and Y. T. Kim, *Sens. Actuators, B*, 2007, **122**, 211–218.
52 B. Zhang, R. W. Fu, M. Q. Zhang, X. M. Dong, P. L. Lan and J. S. Qiu, *Sens. Actuators, B*, 2005, **109**, 323–328.
53 J. Tabačiarová, J. Krajči, J. Pionteck, U. Reuter, M. Omastová and M. Mičušík, *Macromol. Chem. Phys.*, 2016, **217**, 1149–1160.
54 B. Kumar, M. Castro and J.-F. Feller, *Sens. Actuators, B*, 2012, **161**, 621–628.
55 S. Shang, W. Zeng and X.-m. Tao, *Sens. Actuators, B*, 2012, **166**, 330–337.
56 X. Wang, S. Meng, M. Tebyetekerwa, W. Weng, J. Pionteck, B. Sun, Z. Qin and M. Zhu, *Synth. Met.*, 2017, **233**, 86–93.
57 J. Lee, E. J. Park, J. Choi, J. Hong and S. E. Shim, *Synth. Met.*, 2010, **160**, 566–574.
58 S. G. Chen, J. W. Hu, M. Q. Zhang, M. W. Li and M. Z. Rong, *Carbon*, 2004, **42**, 645–651.
59 T. Villmow, A. John, P. Pötschke and G. Heinrich, *Polymer*, 2012, **53**, 2908–2918.
60 S. Chen, W. Ma, Y. Cheng, Z. Weng, B. Sun, L. Wang, W. Chen, F. Li, M. Zhu and H.-M. Cheng, *Nano Energy*, 2015, **15**, 642–653.
61 S. Cavaliere, S. Subianto, I. Savych, D. J. Jones and J. Roziere, *Energy Environ. Sci.*, 2011, **4**, 4761–4785.
62 X. F. Lu, C. Wang, F. Favier and N. Pinna, *Adv. Energy Mater.*, 2017, **7**, 1601301.
63 M. Tebyetekerwa, X. Wang, I. Marriam, P. Dan, S. Yang and M. Zhu, *Mater. Lett.*, 2017, **209**, 400–403.
64 J. Liu, L. Zhang, H. B. Wu, J. Lin, Z. Shen and X. W. D. Lou, *Energy Environ. Sci.*, 2014, **7**, 3709–3719.
65 H. B. Wu, G. Zhang, L. Yu and X. W. Lou, *Nanoscale Horiz.*, 2016, **1**, 27–40.
66 M. Tebyetekerwa, X. Wang, Y. Wu, S. Yang, M. Zhu and S. Ramakrishna, *J. Mater. Chem. A*, 2017, **5**, 21114–21121.
67 Y.-Z. Long, M.-M. Li, C. Gu, M. Wan, J.-L. Duvail, Z. Liu and Z. Fan, *Prog. Polym. Sci.*, 2011, **36**, 1415–1442.

68 P. Kossyrev, *J. Power Sources*, 2012, **201**, 347–352.
69 T. Xu, X. Ding, Y. Liang, Y. Zhao, N. Chen and L. Qu, *Nanoscale*, 2016, **8**, 12113–12117.
70 Y. Meng, Y. Zhao, C. Hu, H. Cheng, Y. Hu, Z. Zhang, G. Shi and L. Qu, *Adv. Mater.*, 2013, **25**, 2326–2331.
71 Y. Hu, H. Cheng, F. Zhao, N. Chen, L. Jiang, Z. Feng and L. Qu, *Nanoscale*, 2014, **6**, 6448–6451.
72 C. Choi, S. H. Kim, H. J. Sim, J. A. Lee, A. Y. Choi, Y. T. Kim, X. Lepró, G. M. Spinks, R. H. Baughman and S. J. Kim, *Sci. Rep.*, 2015, **5**, 9387.
73 X. Chen, L. Qiu, J. Ren, G. Guan, H. Lin, Z. Zhang, P. Chen, Y. Wang and H. Peng, *Adv. Mater.*, 2013, **25**, 6436–6441.
74 Y. Fu, X. Cai, H. Wu, Z. Lv, S. Hou, M. Peng, X. Yu and D. Zou, *Adv. Mater.*, 2012, **24**, 5713–5718.
75 T. Christen and M. W. Carlen, *J. Power Sources*, 2000, **91**, 210–216.
76 W. Ma, S. Chen, S. Yang, W. Chen, Y. Cheng, Y. Guo, S. Peng, S. Ramakrishna and M. Zhu, *J. Power Sources*, 2016, **306**, 481–488.